FOLIA HISTOCHEMICA ET CYTOBIOLOGICA
Vol. 61, No. 2, 2023
pp. 81–97

ORIGINAL PAPER

VIA MEDICA

Immunocytochemical localization of calbindin-D28K, calretinin, and parvalbumin in the Mongolian gerbil (*Meriones unguiculatus*) visual cortex

Jae-Rim Son, Xin-Yu Kuai, Chang-Jin Jeon

Department of Biology, School of Life Sciences, BK21 FOUR KNU Creative BioResearch Group, College of Natural Sciences, and Brain Science and Engineering Institute, and Research Institute for Dok-do and Ulleung-do Island, Kyungpook National University, Daegu, Korea

Abstract

Introduction. While most animals of the *Muridae* family are nocturnal, the gerbil displays diurnal activity and provides a useful model for visual system research. The purpose of this study was to investigate the localization of calcium-binding proteins (CBPs) in the visual cortex of the Mongolian gerbil (*Meriones unguiculatus*). We also compared the labeling of CBPs to those of gamma-aminobutyric acid (GABA)- and nitric oxide synthase (NOS)-containing neurons.

Material and methods. The study was conducted on twelve adult Mongolian gerbils (3–4 months old). We used horseradish peroxidase immunocytochemistry and two-color fluorescence immunocytochemistry with conventional and confocal microscopy to assess CBPs localization in the visual cortex.

Results. The highest density of calbindin-D28K (CB)- (34.18%) and parvalbumin (PV)-IR (37.51%) neurons was found in layer V, while the highest density of calretinin (CR)-IR (33.85%) neurons was found in layer II. The CB- (46.99%), CR- (44.88%), and PV-IR (50.17%) neurons mainly displayed a multipolar round/oval morphology. Two-color immunofluorescence revealed that only 16.67%, 14.16%, and 39.91% of the CB-, CR-, and PV-IR neurons, respectively, contained GABA. In addition, none of the CB-, CR-, and PV-IR neurons contained NOS.

Conclusions. Our findings indicate that CB-, CR-, and PV-containing neurons in the Mongolian gerbil visual cortex are distributed abundantly and distinctively in specific layers and in a small population of GABAergic neurons but are limited to subpopulations that do not express NOS. These data provide a basis for the potential roles of CBP-containing neurons in the gerbil visual cortex. *(Folia Histochemica et Cytobiologica 2023, Vol. 61, No. 2, 81–97)*

Keywords: Mongolian gerbil; visual cortex; calcium-binding proteins; gamma-aminobutyric acid; NOS immunocytochemistry

Introduction

Rats and mice are the two most commonly used small rodents in biomedical research due to their low maintenance costs, high reproductive capacity, and large availability of transgenic strains [1–8]. However, the gerbil, a small mammal in the rodent family, has recently emerged as a useful animal model in several areas of biomedical research owing to its distinctive anatomical and physiological characteristics [9]. For example, the gerbil has been used to study bacterial infection [10], parasitic disease [11–13], hormones [14], the immune system [15], nephropathy [16], type 2 diabetes [17], and cancer [18]. In the field of neuroscience, researchers have also used the gerbil for various studies, notably pertaining to brain development [19], behavior [20], experimental epilepsy [21], ischemia [22–24], memory deficits [25], adaptation to auditory stimulation [26], and early sensory loss [27]. Recently, the genomes of the Mongolian gerbil [28, 29] and the great gerbil [30], along with the mitochondrial genome of the Mongolian gerbil [31] and Tamarisk

Correspondence address:
Prof. Chang-Jin Jeon
Neuroscience Lab., Department of Biology,
College of Natural Sciences,
Kyungpook National University, 80, Daehak-ro, Daegu,
41566, South Korea
phone: +82-53-950-5343, fax: +82-53-953-3066,
e-mail: cjjeon@knu.ac.kr

Folia Histochem Cytobiol. 2023
10.5603/FHC.a2023.0010
ISSN 0239-8508, e-ISSN 1897-5631

gerbil [32], have been sequenced. There have also been recent developments in the generation of gene knockout in the Mongolian gerbil using the CRISPR/ /Cas9 system [33], thus providing novel tools to further advance research.

When studying the visual system, the Mongolian gerbil (*Meriones unguiculatus*) has several advantages over other more commonly used rodents such as rats and mice. In particular, the gerbil's diurnal nature can reveal unique features not found in other Muridae family members with mostly nocturnal lifestyles [19]. Although Mongolian gerbils have rod-dominant retinas like many mammals, they have significantly more retinal cone cells compared to rats and mice [34]. The macula and area centralis are also not present in rats or mice; however, some gerbils have a specialized retinal region like the macular region of primates [35, 36]. These features support the use of gerbils over rats and mice in comparative studies concerning human vision. Therefore, many studies have been undertaken to provide an understanding of aspects of the gerbil's visual system, including multisensory integration in the primary auditory, somatosensory, and visual cortices [37], auditory and visual development during the postnatal stage [38], and outcomes of visual cortical lesions [39]. Other groups have assessed parallel channels for visual orientation [40], changes in supragranular pyramidal neurons in early visual deprivation [27], calretinin (CR)-immunoreactive (IR) neuron distribution in the retina [41], and neuropeptide Y-IR neuron localization in the visual cortex [42].

Calcium is a significant regulatory factor in cellular homeostasis and metabolism. The EF-hand motif-containing calcium-binding proteins (CBPs) calbindin-D28K (CB), calretinin (CR), and parvalbumin (PV) play crucial roles in maintaining proper levels of intracellular calcium ions [43–46]. Many studies have been conducted to unveil the roles of CB, CR, and PV in the central nervous system (CNS). For example, CB was shown to be a significant factor in control of the circadian rhythm [47, 48]. CR is important for the modulation of neuronal excitability and was shown to play a neuroprotective role in diabetic neuropathy [49, 50]. PV modulates intracellular oxidative processes, and PV-positive interneurons of the visual cortex determine multineuronal activity dynamics that increase network synchrony [51, 52]. Although many functions of CBPs are still undetermined, these proteins were found to be distributed abundantly and distinctively in the CNS of various mammalian species. Abundant CB-, CR-, and PV-expressing neurons show distinctive distributional patterns in the visual cortices of animals, including mice [53], hamsters [54], bats [55], rats [56], rabbits [57], cats [58], dogs [59], monkeys [60, 61], and humans [62, 63].

Nitric oxide (NO) is a gaseous molecule and an important neurotransmitter synthesized from L-arginine by the enzyme NO synthase (NOS), activation of which requires Ca^{2+} influx [64, 65]. NOS has three isozymes: neuronal NOS in neurons, inducible NOS in macrophages, and endothelial NOS in endothelial cells [66]. Neuronal NOS plays many important roles in the nervous system, including neurotransmission, synaptic plasticity, neurogenesis, and learning and memory [67, 68]. Neuronal NOS is also related to neurodegenerative diseases such as Alzheimer's disease, Parkinson's disease, and Huntington's disease [69–71]. Neuronal NOS is present in both the peripheral nervous system and CNS, including various visual areas, such as the visual cortex and superior colliculus [54, 56, 72–81]. NOS is activated through calmodulin by elevated intracellular calcium ion levels [82, 83]. CBPs play important roles in maintaining intracellular calcium ion levels in the CNS. Therefore, the relationship between NOS and CBPs has been extensively studied [56, 84–88]. For example, in the rat neocortex, CB, CR, and PV are absent or found at very low levels in NOS-containing neurons [89], whereas, in the rat cerebral cortex, 24–34% of CB-containing cells also contained NOS [84, 85]. A minority of CB, CR, and PV-containing neurons also contained NOS in the rat claustrum [75], and in the hippocampi of mice and rats, some CR-containing cells also contained NOS [86, 87]. Small cell body-sized NOS-containing neurons often colocalized with CB but not with CR or PV in the human temporal cortex [90].

Currently, the distribution of CB-, CR-, and PV-containing neurons in the gerbil visual cortex is unknown. We have conducted a comprehensive study of these neurons in the visual cortex to provide a better understanding of gerbil vision. The first goal of our study was to assess the distribution and morphology of CB-, CR-, and PV-IR neurons quantitatively, using immunocytochemistry, brightfield microscopy, and confocal microscopy. Next, we examined whether CB-, CR-and PV-IR neurons express gamma-aminobutyric acid (GABA), as many CBP-containing neurons are GABAergic interneurons in other areas of the brain [56, 72, 91, 92]. Finally, we examined whether CBP-IR neurons express NO, which is associated with elevated intracellular calcium concentration.

Material and methods

Animals and tissue preparation. Twelve Mongolian gerbils (*Meriones unguiculatus*), all 3–4 months old and weighing

Folia Histochem Cytobiol. 2023
10.5603/FHC.a2023.0010
ISSN 0239-8508, e-ISSN 1897-5631

70–90 g, were obtained from an in-house breeding facility for use in this study. Animals were group housed under a 12-h light:12-h dark cycle until use. Temperature and humidity levels in animal housing facilities ranged from 23°C to 26° and from 45% to 65%, respectively. The animals were anesthetized by isoflurane inhalation (1.5% in 70% nitrous oxide), then perfused intracardially with approximately 10 mL of phosphate-buffered saline (PBS, pH 7.4) over a period of 3 min, followed by 30 mL of fixative (4% paraformaldehyde and 0.3–0.5% glutaraldehyde in 0.1 M PBS containing 0.002% calcium chloride) over 20–30 min, using a syringe needle inserted through the left ventricle and aorta. The extracted brains were postfixed overnight and then cut into 50 μm coronal sections using a Vibratome 3000 Plus Sectioning System (Vibratome, St. Louis, MO, USA). All animal experiments were approved by the committee of Kyungpook National University (permission NO. 2021-0072). Guide for the Care and Use of Laboratory Animals (https://grants.nih.gov/grants/olaw/guide-for-the-care-and-use-of-laboratory-animals.pdf) was followed.

Horseradish peroxidase (HRP) immunocytochemistry. The primary antibodies used in this study were as follows: mouse anti-CB (Sigma-Aldrich, St. Louis, MO, USA), mouse anti-CR (Millipore, Burlington, MA, USA), and mouse anti-PV (Sigma--Aldrich). The primary antibodies were diluted 1:500. Tissues were processed free-floating in small vials at room temperature with gentle agitation. For immunocytochemistry, the tissues were incubated in 1% sodium borohydride (NaBH4) for 30 min. Afterward, the tissues were rinsed for 3 × 10 min in PBS, then incubated in PBS with 4% normal horse serum (Vector Laboratories, Burlingame, CA, USA) with 0.5% Triton X-100 for 2 h. Next, the tissues were incubated for 24 h with primary antibodies diluted 1:500 in PBS containing 4% normal serum with 0.5% Triton X-100. After three 10-minute rinses with PBS, the tissues were incubated in a 1:200 dilution of biotinylated secondary goat anti-mouse IgG (Vector Laboratories) in a blocking solution. The tissues were again rinsed for 3 × 10 min in PBS, then incubated in a 1:50 dilution of avidin-biotinylated horseradish peroxidase complex (Vector Laboratories) in PBS for 2 h. Next, tissues were rinsed in 0.25 M Tris buffer for 3 × 10 min. Finally, staining was visualized by reaction with 1,3'-diaminobenzidine tetrahydrochloride (DAB) and hydrogen peroxide in 0.25 M Tris buffer for 30–60 sec using a DAB reagent kit (Seracare, Milford, MA, USA). All tissues were then rinsed in 0.25 M Tris buffer before mounting. As a negative control, some sections were incubated in the same solutions without the addition of the primary antibodies, and these control tissues exhibited no immunoreactivity. After the immunocytochemical staining, the tissues were mounted on Superfrost Plus slides (Fisher, Pittsburgh, PA, USA) and dried overnight in a 37°C oven. The mounted sections were dehydrated with alcohol, cleared with xylene, and then coverslips were applied with Permount (Fisher). The tissues were examined and photographed on a Zeiss Axioplan microscope (Carl Zeiss Meditec Incorporation, Jena, Germany) using conventional or differential interference contrast (DIC) optics.

Fluorescence immunocytochemistry. For the double-labeling of CBPs and GABA, the primary antibodies used in this study were as follows: mouse anti-GABA (Millipore), rabbit anti-CB (Sigma-Aldrich), rabbit anti-CR (Millipore), and rabbit anti-PV (Sigma-Aldrich). For the double-labeling of CBPs and NOS, the primary antibodies used were mouse anti-NOS (BD biosciences, San Jose, CA, USA), mouse anti-CB (Sigma-Aldrich), mouse anti-CR (Millipore), and mouse anti-PV (Sigma-Aldrich). The primary antibodies were diluted either 1:400 (GABA), 1:200 (NOS), or 1:200-1:500 (CB, CR, and PV). For the staining of CB, CR, and PV, the secondary antibodies were fluorescein (FITC)-conjugated anti-rabbit IgG (Vector Laboratories) or FITC-conjugated anti-mouse IgG (Vector Laboratories). A Cy3-conjugated anti-mouse IgG (Jackson ImmunoResearch Inc, Baltimore, PA, USA) secondary antibody was used to identify GABA and NOS. Labeled sections were preserved under coverslips in the Vectashield mounting medium (Vector Laboratories).

Quantitative analysis. The laminal distribution of the CB-, CR-, and PV-IR neurons were examined in three different 500 μm sections from each of the three animals (9 sections total). Imaging was conducted using a Zeiss Axioplan microscope (AxioVision 4; Carl Zeiss Meditec Inc.). Double-labeled neurons stained for GABA and CBPs were counted in three different 500 μm sections from each of the three animals (9 sections total). Double-labeled neurons stained for NOS and CBPs were counted in three different 1,000 μm sections from each of the three animals (9 sections total). Double-labeled images were obtained on a Zeiss LSM800 laser scanning confocal microscope (Carl Zeiss Meditec Inc.) using a 40× objective. The morphological types of CB-, CR-, and PV-IR neurons were further analyzed from fluorescence-stained or DAB-reacted sections. Fluorescence images were photographed with a Zeiss LSM800 laser scanning confocal microscope (Carl Zeiss Meditec Inc.) using a 40× objective. DIC images were acquired with a Zeiss Axioplan microscope (AxioVision 4; Carl Zeiss Meditec Inc.) using 40× or 63× objectives.

Results

Distribution of CBP- immunoreactive (IR) neurons

As shown in Fig. 1, the laminar distribution of CB- (Fig. 1B), CR- (Fig. 1C), and PV- (Fig. 1D) IR neurons was first examined. Thionin staining was used to visualize cortical lamination (Fig. 1A). Fig. 1E shows the distribution of GABA-IR neurons. Each type of CBP-IR neuron was found to be distributed differently in the gerbil visual cortex. The highest density of CB-IR neurons was observed in layer V. The quantitative histogram of the cell distribution shown

Folia Histochem Cytobiol. 2023
10.5603/FHC.a2023.0010
ISSN 0239-8508, e-ISSN 1897-5631

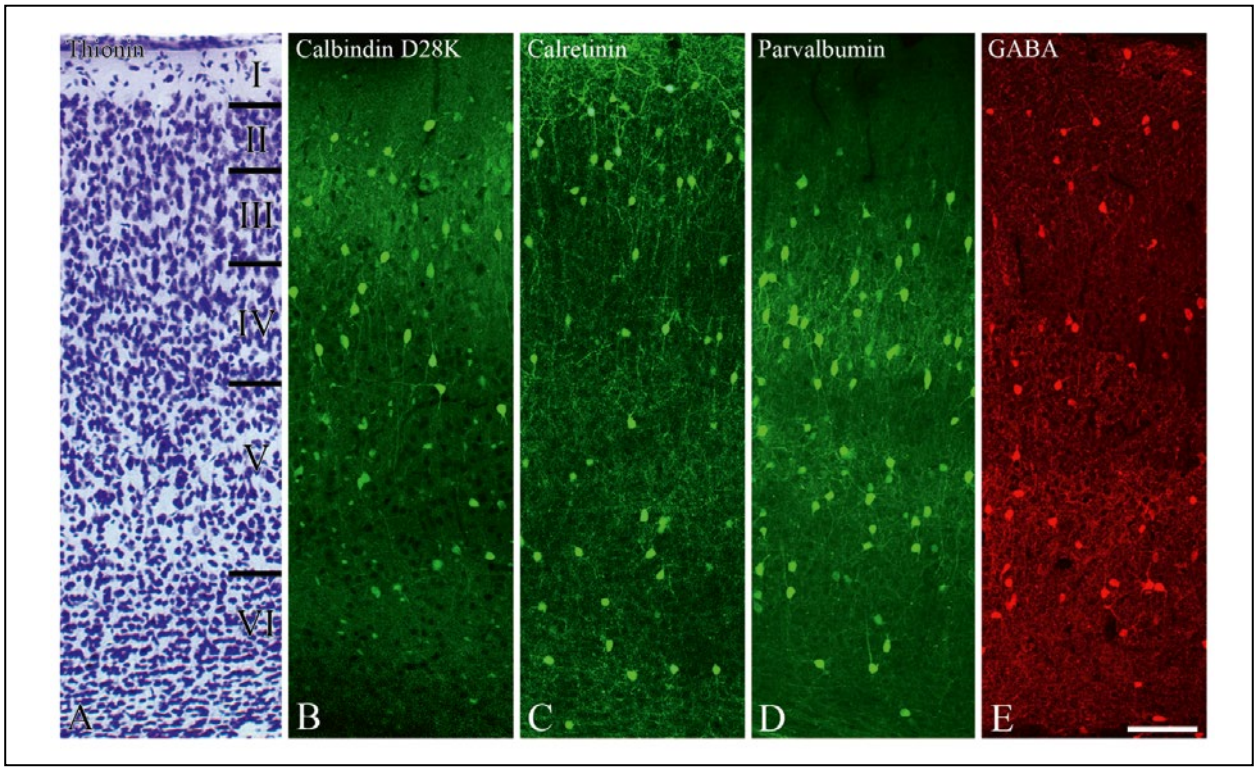

Figure 1. Low-power photomicrographs showing the laminal distribution of calcium-binding proteins (CBPs) and GABA-IR neurons in the gerbil visual cortex. **A.** Thionin-stained section illustrating cortical lamination. **B.** CB-IR neurons. **C.** CR-IR neurons. **D.** PV-IR neurons. **E.** GABA-IR neurons. Abbreviations: CB — calbindin-D28K; CR — calretinin; GABA — gamma-aminobutyric acid; IR — immunoreactive; PV — parvalbumin. Scale bar = 100 μm.

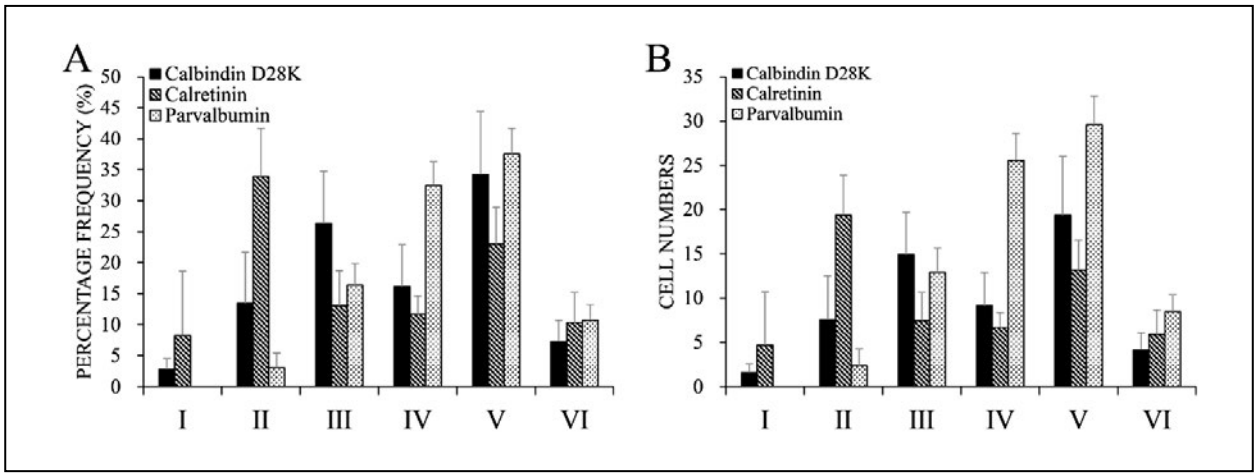

Figure 2. Histogram showing the distribution of CBP-IR neurons in the gerbil visual cortex. The density of CB-IR neurons is highest in layer V, whereas CR-IR neurons are predominantly located in layer II. The majority of PV-IR neurons were found in layers IV–V, but none were observed in layer I. Abbreviations as in the description of Fig. 1.

in Fig. 2 shows the density of CB-IR neurons in each cortical layer: 2.75% (1.56 cells on average) of labeled neurons were found in layer I, 13.36% (7.56 cells on average) in layer II, 26.33% (14.89 cells on average) in layer III, 16.11% (9.11 cells on average) in layer IV, 34.18% (19.33 cells on average) in layer V, and 7.27% (4.11 cells on average) in layer VI. The highest density of CR-IR neurons was observed in layer II. The quantitative histogram of the cell distribution provided in Fig. 2 shows the density of CR-IR neurons in each layer: 8.17% (4.67 cells on average) of labeled neurons were found in layer I, 33.85% (19.33 cells on average) in layer II, 13.04% (7.44 cells on average) in layer III, 11.67% (6.67 cells on average) in layer IV, 22.96% (13.11 cells on average) in layer V, and 10.31% (5.89 cells on average) in layer VI. The PV-IR neurons

Folia Histochem Cytobiol. 2023
10.5603/FHC.a2023.0010
ISSN 0239-8508, e-ISSN 1897-5631

were predominantly located in layers IV and V, with none found in layer I. The quantitative histogram of the cell distribution provided in Fig. 2 shows the density of the PV-IR neurons in each layer: 0.00% of labeled neurons were found in layer I, 2.96% (2.33 cells on average) in layer II, 16.36% (12.89 cells on average) in layer III, 32.44% (25.56 cells on average) in layer IV, 37.51% (29.56 cells on average) in layer V, and 10.72% (8.44 cells on average) in layer VI.

Morphology of CB-IR neurons

The CB-IR neurons displayed various shapes in the gerbil visual cortex, including multipolar round/oval, vertical fusiform, multipolar stellate, horizontal, pyriform, and Martinotti types (Fig. 3). Most CB-IR neurons in the gerbil visual cortex were found to be round/oval. Fig. 3A shows a multipolar cell type with a round/oval cell body and multiple processes. Fig. 3B shows a stellate type, displaying a polygonal-shaped cell body with extending dendrites in various directions. Some of the CB-IR multipolar stellate neurons also had varicosities (arrowheads in Fig. 3B). Fig. 3C shows a pyriform type with a pyriform cell body and a bouquet of dendrites directed toward the pial surface. Fig. 3D shows a horizontal type, with a horizontally oriented cell body and dendrites. Fig. 3E shows a vertical fusiform type, presenting a vertical fusiform cell body with a long main process ascending toward the pial surface and another descending process. Fig. 3F shows a Martinotti cell type displaying a long process toward the pial surface and some dendrites stretching sideways. Quantitatively, 46.99% ± 3.51% (156 of 332 cells) of CB-IR neurons were of the multipolar round/ /oval type, 16.87% ± 5.15% (56 of 332 cells) were of the multipolar stellate type, 21.39% ± 4.60% (71 of 332 cells) were of the vertical fusiform type, 3.01% ± ± 2.50% (10 of 332 cells) were of the horizontal type, 11.45% ± 3.20% (38 of 332 cells) were of the pyriform type, and 0.30% ± 0.72% (1 of 332 cells) were of the Martinotti type (Fig. 4).

Morphology of CR-IR neurons

The CR-IR neurons also varied in shape within the gerbil visual cortex, displaying multipolar round/ /oval, vertical fusiform, multipolar stellate, horizontal, and pyriform cell morphologies (Fig. 5). Most CR-IR neurons were of the multipolar round/oval (Figs. 5A, 5B, arrowhead in 5C) and vertical fusiform (arrow in Figs. 5C, 5D) types. The multipolar round/oval cells had several dendrites extending in various directions. Some CR-IR round/oval neurons also had varicosities (enlarged box in Fig. 5A). The arrows in Figs. 5C and 5D indicate a vertical fusiform type, which displays a vertical fusiform cell body with a process ascending toward the pial surface as well as a descending process. The stellate types shown in Figs. 5E and 5F had several dendrites oriented in various directions. Fig. 5G provides an example of a pyriform type with a pyriform cell body and a dendrite directed toward the pial surface. Some horizontal-type cells, with horizontal fusiform cell bodies and horizontally oriented processes, also contained CR (Fig. 5H). Quantitatively, 44.88% ± ± 4.52% (136 of 303 cells) of CR-IR neurons were of the multipolar round/oval type, 12.87% ± 5.23% (39 of 303 cells) were of the multipolar stellate type, 31.02% ± 5.49% (94 of 303 cells) were of the vertical fusiform type, 1.32% ± 1.72% (4 of 303 cells) were of the horizontal type, and 9.90% ± 5.04% (30 of 303 cells) were of the pyriform type (Fig. 4).

Morphology of PV-IR neurons

The PV-IR neurons also consisted of various shapes in the gerbil visual cortex, resulting in multipolar round/ /oval, vertical fusiform, multipolar stellate, horizontal, pyriform, and Martinotti cell types (Fig. 6). Most PV-IR neurons that we observed were round/oval. Figs. 6A and 6B show representative multipolar round/oval cells with round/oval cell bodies and many dendrites coursing in different directions. Fig. 6C shows a vertical fusiform cell displaying a vertical fusiform cell body with an ascending process toward the pial surface and another descending process. Fig. 6D shows a stellate type, presenting a polygonal-shaped cell body and many dendrites coursing in several directions. Fig. 6E provides an example of a pyriform type, with a pyriform cell body and thick, proximal dendrites directed toward the pial surface. Fig. 6F illustrates a horizontal type, with a horizontally oriented cell body and dendrites. Fig. 6G shows a Martinotti type displaying a long process toward the pial surface and some dendrites stretching sideways. Quantitatively, 50.17% ± 7.97% (147 of 293 cells) of PV-IR neurons were of the multipolar round/oval type, 16.72%± ± 6.51% (49 of 293 cells) were of the multipolar stellate type, 20.82% ± 3.68% (61 of 293 cells) were of the vertical fusiform type, 1.02% ± 1.37% (3 of 293 cells) were of the horizontal type, 10.92% ±5.23% (32 of 293 cells) were of the pyriform type, and 0.34% ± 1.23% (1 of 293 cells) were of the Martinotti type (Fig. 4).

Colocalization of CBPs and GABA

We next determined whether CB-, CR-and PV-IR neurons in the gerbil visual cortex co-localized with GABA. While some neurons were clearly labeled by both anti-GABA and an anti-CBP antibody, other neurons were labeled only by one or the other (Fig. 7, Table 1). Fig. 7 shows neurons labeled for CBPs (Figs. 7A, D, G), GABA (Figs. 7B, E, H), and

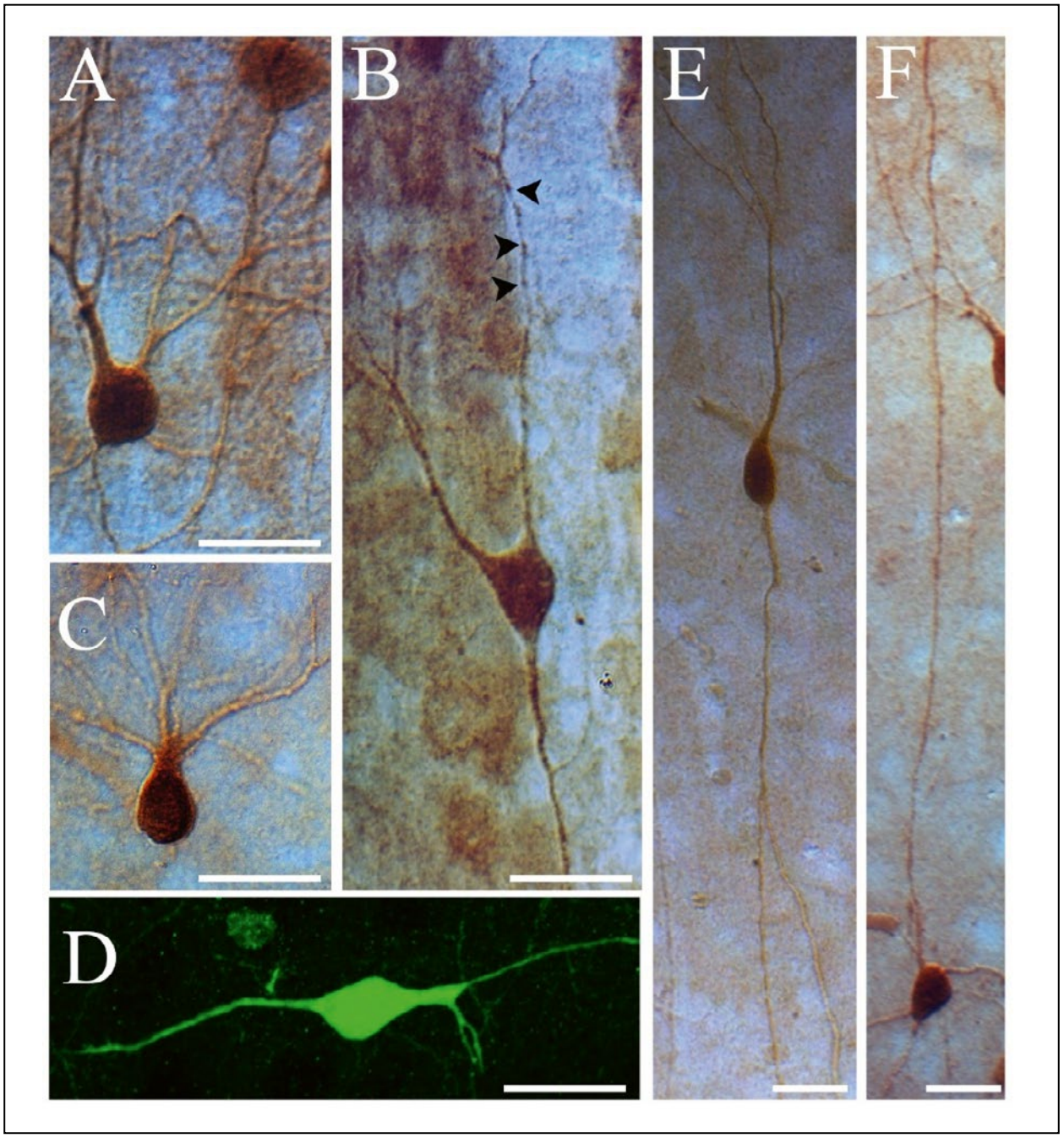

Figure 3. High-power DIC and fluorescence photomicrographs revealing the morphology of calbindin-IR neurons in the gerbil visual cortex. **A.** Multipolar round/oval type. **B.** Multipolar stellate type with multiple processes with varicose fibers (arrowheads). **C.** Pyriform type with a bouquet of dendrites. **D.** Horizontal type with a fusiform cell body extending horizontally oriented processes. **E.** Vertical fusiform type with cell body extending vertically oriented processes. **F.** Martinotti type with processes ascending toward the pial surface. Abbreviations: CB — calbindin-D28K; DIC — differential interference contrast; IR — immunoreactive. Scale bar = 20 μm.

the superimposition of combined CBP and GABA staining (Figs. 7C, F, I). Arrowheads in Figs. 7C, F, and I show neurons with colocalization of CBP and GABA. Quantitatively, 16.67% ± 2.90% (75 of 450 cells) of CB-IR neurons were double-labeled with GABA, 14.16% ± 2.58% (63 of 445 cells) of CR-IR neurons were double-labeled with GABA, and 39.91% ± 6.61% (269 of 674 cells) of PV-IR neurons were double-labeled with GABA (Table 1).

Colocalization of CBPs and NOS

Finally, we assessed whether CB-, CR-and PV-IR neurons in the gerbil visual cortex colocalized with NOS. Fig. 8 shows neurons labeled with CBPs

Folia Histochem Cytobiol. 2023
10.5603/FHC.a2023.0010
ISSN 0239-8508, e-ISSN 1897-5631

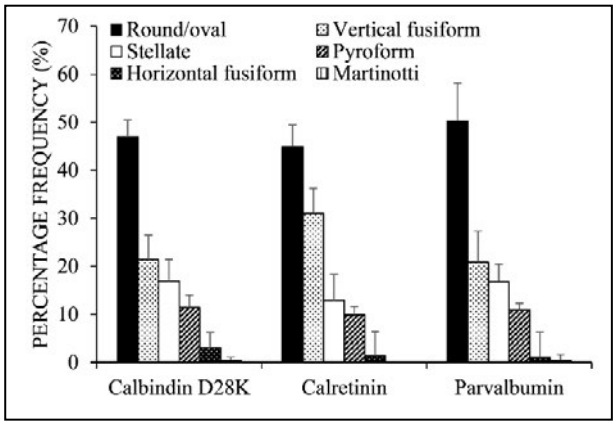

Figure 4. Histogram showing the distribution of morphologically different types of neurons labeled by CBPs in the gerbil visual cortex. The major types of CB-, CR-, and PV-IR neurons are multipolar round/oval cells. Many other CR-IR neurons are vertical fusiform cells. Martinotti cells were the least commonly observed type for CB- and PV-IR neurons. Abbreviations as in the description of Fig. 1.

(Figs. 8A, D, G), NOS (Figs. 8B, E, H), and the superimposition of images stained for both (Figs. 8C, F, I). None of the CB-, CR-, and PV-IR cells coexpressed NOS (Figs. 8C, F, I, Table 1).

Discussion

Our results demonstrate that CB, CR, and PV are contained within various types of neurons in the gerbil visual cortex, with the three CBPs displaying differential laminal distribution. Compared to the numbers reported for other animals by other studies, fewer CBP neurons express GABA in the gerbil visual cortex, and none contain NOS.

The density of CB-IR neurons in the gerbil visual cortex was the highest in layer V. This distribution pattern is very similar to previous descriptions in mice [53], hamsters [54], rats [56], and rabbits [57]. However, the distribution pattern of CB-IR neurons in the gerbil visual cortex significantly differs from flying foxes [93], cats [94], dogs [59], monkeys [60, 95], and humans [63], in which CB-IR neurons are mostly II distributed in layer II–III, and bats [55], in which CB-IR neurons are most abundant in layer IV. The highest density of CR-IR neurons in the gerbil visual cortex was observed in layer II. Unlike CB-IR neurons, the distribution of CR-IR neurons displays a similar pattern among many mammals, showing the highest density in layers II/III of the visual cortex in gerbils (current study), mice [53], hamsters [54], bats [55], rats [56], rabbits [57], cats [58], monkeys [61], and humans [62]. Most PV-IR neurons in the gerbil visual cortex were distributed in layers IV–V, without any PV-IR neurons observed in layer I. Similarly, PV--IR neurons are mostly distributed in layer IV in bats [55], rats [56], cats [96], monkeys [60], and humans [63]. Although not drastically different, most PV-IR neurons in the visual cortices of hamsters and mice

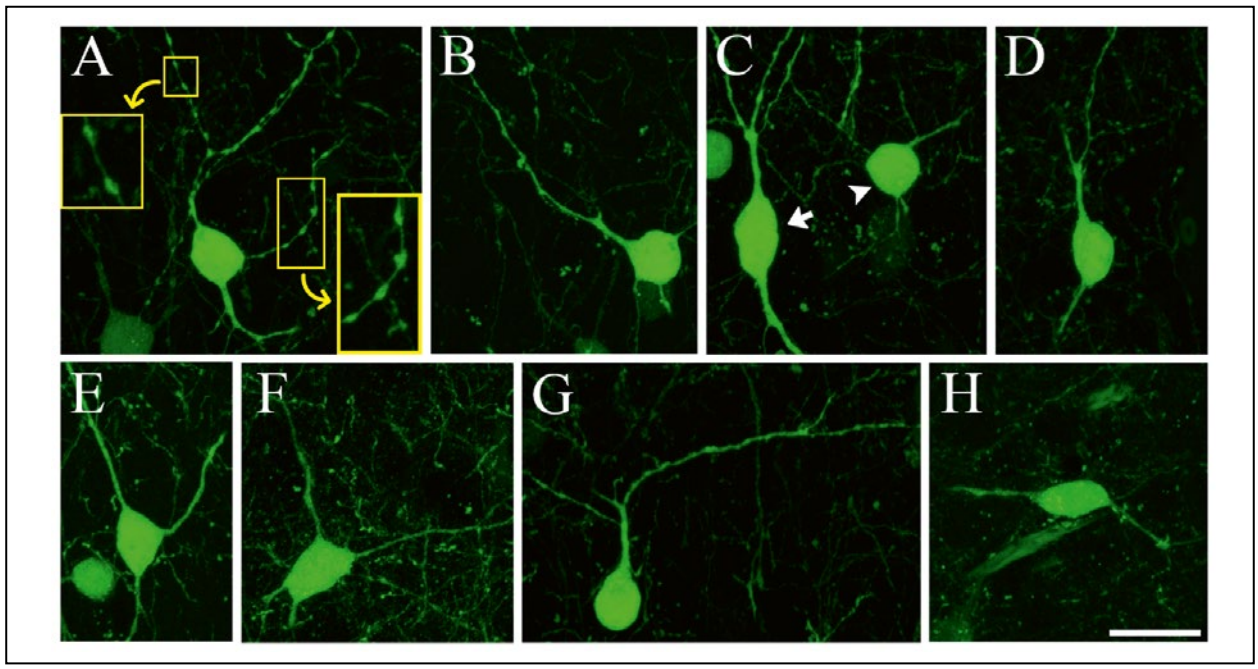

Figure 5. Fluorescence photomicrographs revealing the morphology of calretinin-IR neurons in the gerbil visual cortex. **A.** Multipolar round/oval type with varicose fibers, enlarged in box. **B.** Round/oval type. **C.** Fusiform type with vertically oriented cell body and processes (arrow), as well as round/oval type (arrowhead). **D.** Vertical fusiform type with vertically oriented cell body and processes. **E, F.** Multipolar stellate type. **G.** Pyriform type with a dendrite directed toward the pial surface. **H.** Horizontal fusiform type with horizontally oriented cell body and processes. Abbreviations as in the description of Fig. 1. Scale bar = 20 μm.

Folia Histochem Cytobiol. 2023
10.5603/FHC.a2023.0010
ISSN 0239-8508, e-ISSN 1897-5631

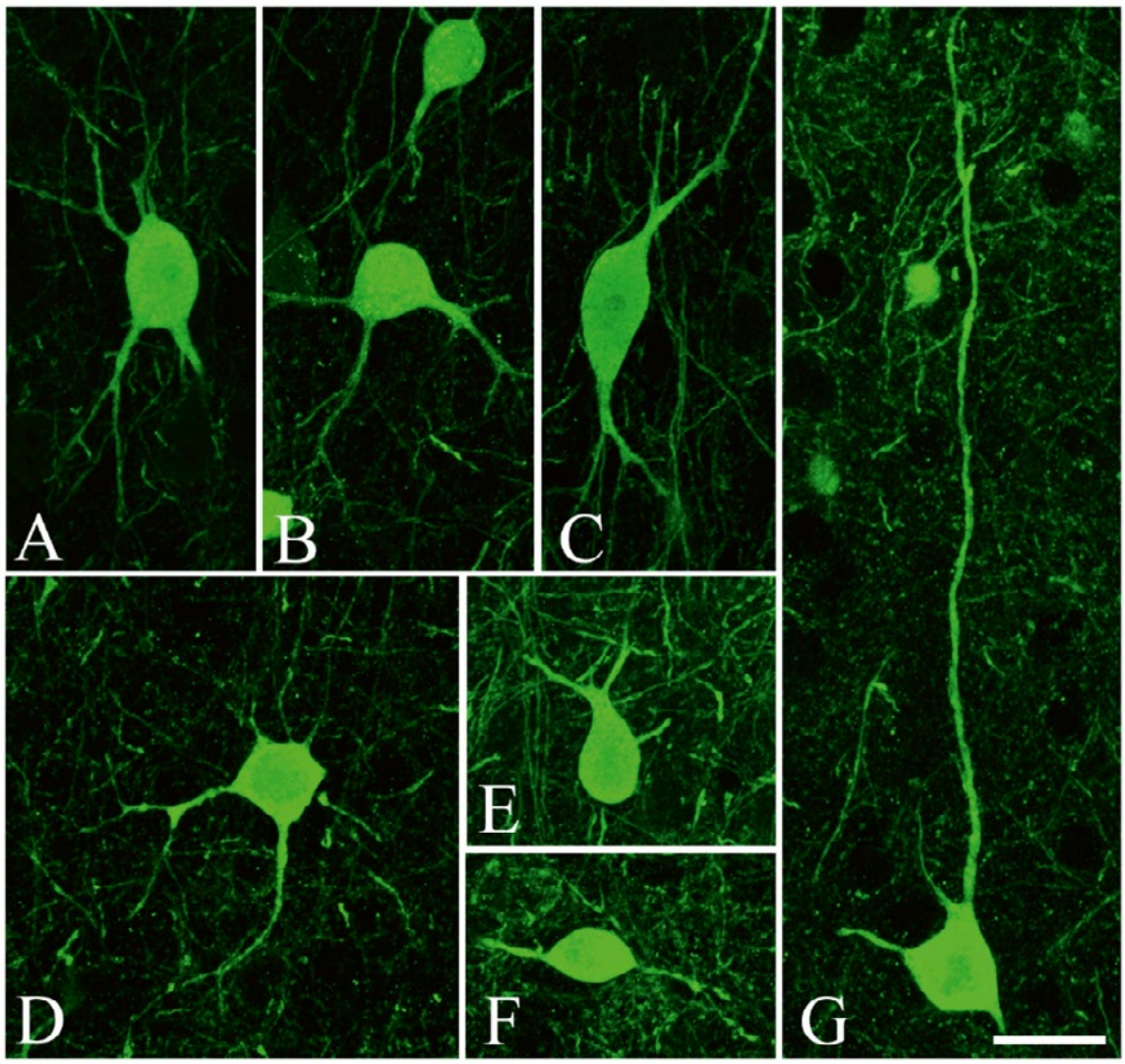

Figure 6. Fluorescence photomicrographs revealing the morphology of parvalbumin-IR neurons in the gerbil visual cortex. **A, B.** Multipolar round/oval type. **C.** Fusiform type with a vertically oriented cell body and processes. **D.** Multipolar stellate type with multiple processes. **E.** Pyriform type with a pyriform cell body and a thick dendrite directed toward the pial surface. **F.** Horizontal type with a horizontally oriented cell body and processes. **G.** Martinotti type with a process ascending toward the pial surface. Abbreviations as in the description of Fig. 1. Scale bar = 20 μm.

are distributed in layers IV–VI [97]. Diverging further, PV-IR neurons are mostly distributed in layers II–VI of New World monkey and Marmoset visual cortices [95], and in layers III–VI in rabbits [57]. Thus, although CBPs display some common laminar distribution patterns between species, unique patterns can also be found. The functional significance of these unique, species-specific laminar distribution patterns is unknown. In addition, considering that each visual cortical layer performs different functions, subtle differences in their structural and functional connectivity associated with CBP-containing neurons will be an important area of future exploration.

In the gerbil visual cortex, the major type of CB-IR neurons was round/oval. Similarly, in the visual cortices of mice [53], hamsters [54], bats [55], rats [56], flying foxes [93], rabbits [57], cats [94], dogs [59], monkeys [60], and humans [63], the predominant types of CB-IR neurons are stellate and round/oval cells. In the gerbil visual cortex, most CR-IR neurons were round/oval, followed by vertical fusiform, like those identified in many other animals. In mice [53] and rabbits [57], most CR-IR neurons in the visual cortex are also fusiform. In the visual cortex of hamsters [54], bats [55], rats [56], cats [58], dogs [59], monkeys [60], dolphins [62], and humans [63], the main type of CR-IR neurons were round/oval and vertical fusiform.

Folia Histochem Cytobiol. 2023
10.5603/FHC.a2023.0010
ISSN 0239-8508, e-ISSN 1897-5631

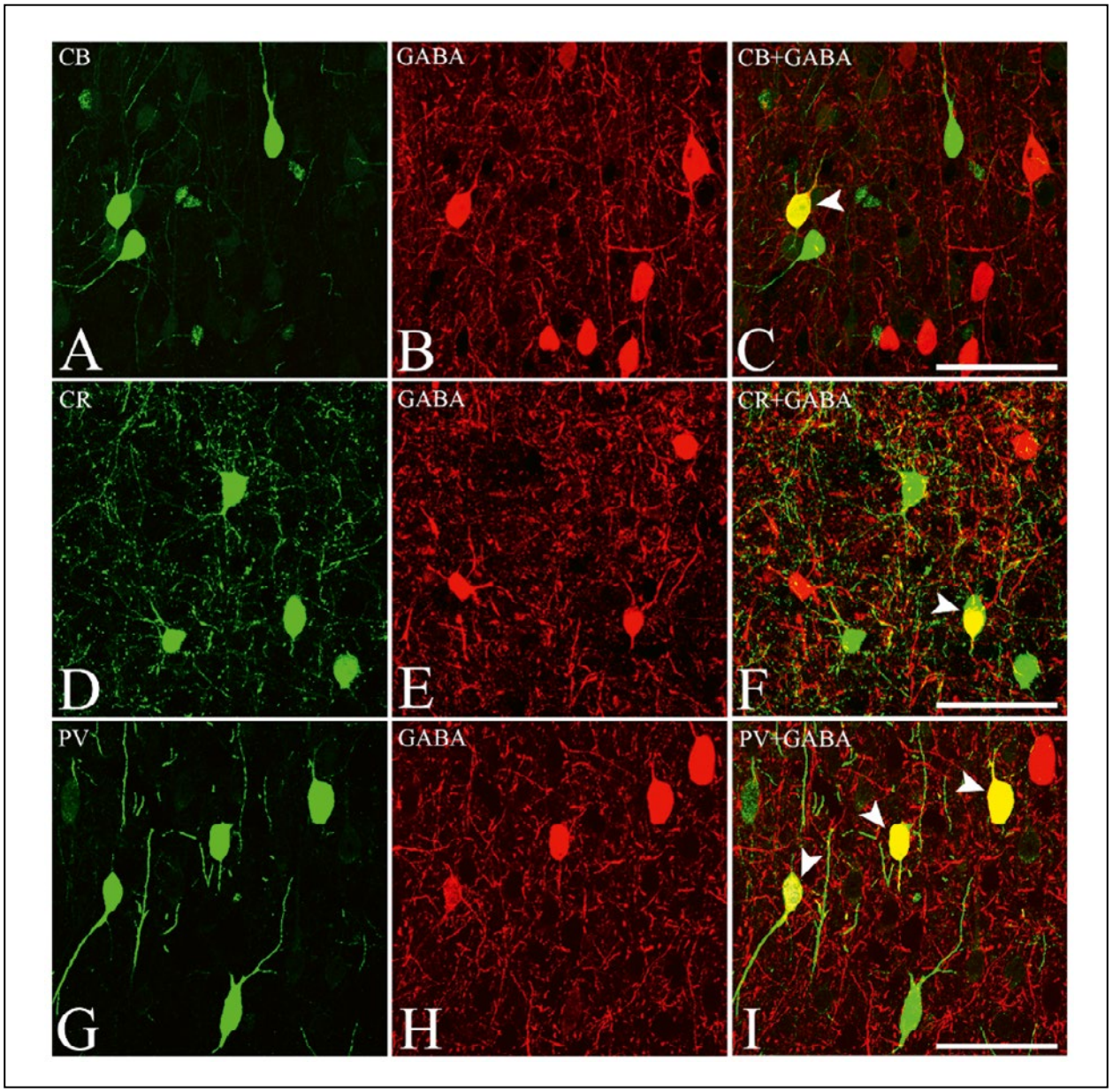

Figure 7. Fluorescence confocal photomicrographs of the gerbil visual cortex immunostained for calcium-binding proteins (CBPs) (A, D, G) or GABA (B, E, H), and superimposed images of CBP and GABA staining (C, F, I). Some of the CB-IR (arrowhead in C), CR-IR (arrowhead in F), and PV-IR (arrowhead in I) neurons are double-labeled with GABA. Abbreviations as in the description of Fig. 1. Scale bar = 50 μm.

The predominant type of PV-IR neurons in the gerbil visual cortex was round/oval, like those identified in mice and hamsters [97], bats [55], rats [56], rabbits [57], cats [94], dogs [59], monkeys [60, 98], and humans [98]. In addition to the round/oval, stellate, and vertical fusiform types of cells, a few pyriform and horizontal fusiform cells were also found to contain CB, CR, and PV. Martinotti cell morphology was also found rarely in CB- and PV-IR neurons. These results align with previous studies showing a similar organization and suggest that these neurons are nonpyramidal interneurons [99, 100]. However, CBP-IR neurons consist of both pyramidal and nonpyramidal neurons in some species. For example, in the human neocortex, CB-IR neurons represent a large population of pyramidal neurons [101]. In the cat visual cortex, only a few CB-IR neurons were pyramidal neurons [94]. In the visual systems of other species, some CB-, CR-, and PV-IR cells were projection neurons. For example, many retinal ganglion cells are CB- [102], CR- [103, 104], or PV-IR neurons [105, 106], and a significant proportion of CB-IR neurons in the cat superior

Table 1. Quantitative analysis of CBP-IR neurons colocalized with GABA and NOS in the Mongolian gerbil visual cortex

Antibody		Width per Section	No. of Sections	No. of CBP-IR Cells	No. of double IR	% double IR (Mean ± SD)
GABA	calbindin-D28K	500 μm	9	450	75	16.67 ± 2.90
	calretinin	500 μm	9	445	63	14.16 ± 2.58
	parvalbumin	500 μm	9	674	269	39.91 ± 6.61
NOS	calbindin-D28K	1,000 μm	9	922	0	0.00 ± 0.00
	calretinin	1,000 μm	9	982	0	0.00 ± 0.00
	parvalbumin	1,000 μm	9	1466	0	0.00 ± 0.00

Abbreviations: CBP — calcium-binding protein; GABA — gamma-aminobutyric acid; IR — immunoreactive; NOS — nitric oxide synthase; SD — standard deviation.

colliculus [4] are projection neurons. The localization of CBPs not only in interneurons but also in projection neurons depending on brain location and species might suggest the functional and connectional diversity of CBP-containing neurons.

In the gerbil visual cortex, some CB-IR multipolar stellate and some CR-IR multipolar round/oval neurons had varicose fibers. In the visual system, for example, varicosities are notably found in CB-IR multipolar stellate neurons from the cat [4] and dog superior colliculus [107]. CR-IR multipolar stellate neurons are found in the rabbit [108] and dog superior colliculus [109], and PV-IR multipolar stellate neurons are found in the hamster visual cortex [97]. The varicosities observed in specific subtypes of CB- and CR-IR neurons in the present study might suggest their involvement in subtly distinct roles. Although the function of dendritic varicosities is still not fully understood, it is known that amacrine dendritic varicosities electrically isolate local input-output neuronal circuits [110]. Axonal varicosities, which are involved in the antidromic propagation of action potentials to the soma in a retrograde manner [111], likely play a role in neuron mechanosensation [112] and protection [113] in the CNS, and contribute to blood flow regulation in the peripheral nervous system [114]. The observed varicosities suggest the activation of neurons. When visual or electrical stimulation was performed at cholinergic fibers from the horizontal diagonal band of Broca projecting to the prefrontal cortex, the density of choline acetyltransferase-IR varicosities on activated pyramidal neurons of the prefrontal cortex was significantly increased compared with nonactivated pyramidal neurons in the stimulation group or control rats [115]. Thus, the varicosity-containing CB- and CR-IR neurons may play key roles in the differential encoding of visual signals and in regulating the conduction of synaptic potentials locally.

The present study also showed that some CB-, CR-, and PV-IR neurons in the gerbil visual cortex also contained GABA. The relatively low percentage of neurons double-labeled for GABA and CBPs is surprising, given that the morphologies of CB-, CR-, and PV-IR neurons were nonpyramidal, and many reports have found high percentages of CB-, CR-, and PV-IR in GABAergic neurons of the visual cortex. However, in our experiment we consistently found a low percentage of neurons double-labeled with GABA, suggesting differences in double-labeling are clear even among rodent species. Contrary to the present result, 100% of CR-IR neurons and 100% of PV-IR neurons express GABA in the mouse visual cortex [72], and 97% of CB-IR neurons, 94% of CR-IR neurons, and 100% of PV-IR neurons express GABA in the rat visual cortex [56]. Additionally, 95% of CR-IR neurons express GABA in the monkey visual cortex [61], whereas 80% of CR-IR and 93% of PV-IR neurons express GABA in the cat visual cortex [96]. Varying slightly, 66% of CB-IR neurons, 92% of CR-IR neurons, and 96% of PV-IR neurons express GABA in the dog visual cortex [59]. In the bat visual cortex, 66% of CB-IR neurons, 24% of CR-IR neurons, and 77% of PV-IR neurons express GABA [55]. However, the present results indicate that most CBP-IR neurons are not GABA-containing interneurons in the gerbil visual cortex.

The double-labeling ratio of CBPs and GABA also significantly differs based on the brain area. For example, in the mouse superior colliculus [116], 36% of PV-IR neurons in the superficial layer and 81% of PV-IR neurons in the intermediate layer contain GABA. In the bat superior colliculus [117], CB-IR neurons and CR-IR neurons do not stain for GABA, but 10.27% of PV-IR neurons do. Only 4% of CB-IR neurons express GABA in the cat's superior colliculus [4], and CR-IR neurons in its superficial layers do not contain GABA [118]. In the dog superior colliculus, no CR-IR neurons express GABA, but 11.20% of CB-IR neurons and 11.67% PV-IR neurons do [107, 109, 119]. These results illustrate that there are variable

Folia Histochem Cytobiol. 2023
10.5603/FHC.a2023.0010
ISSN 0239-8508, e-ISSN 1897-5631

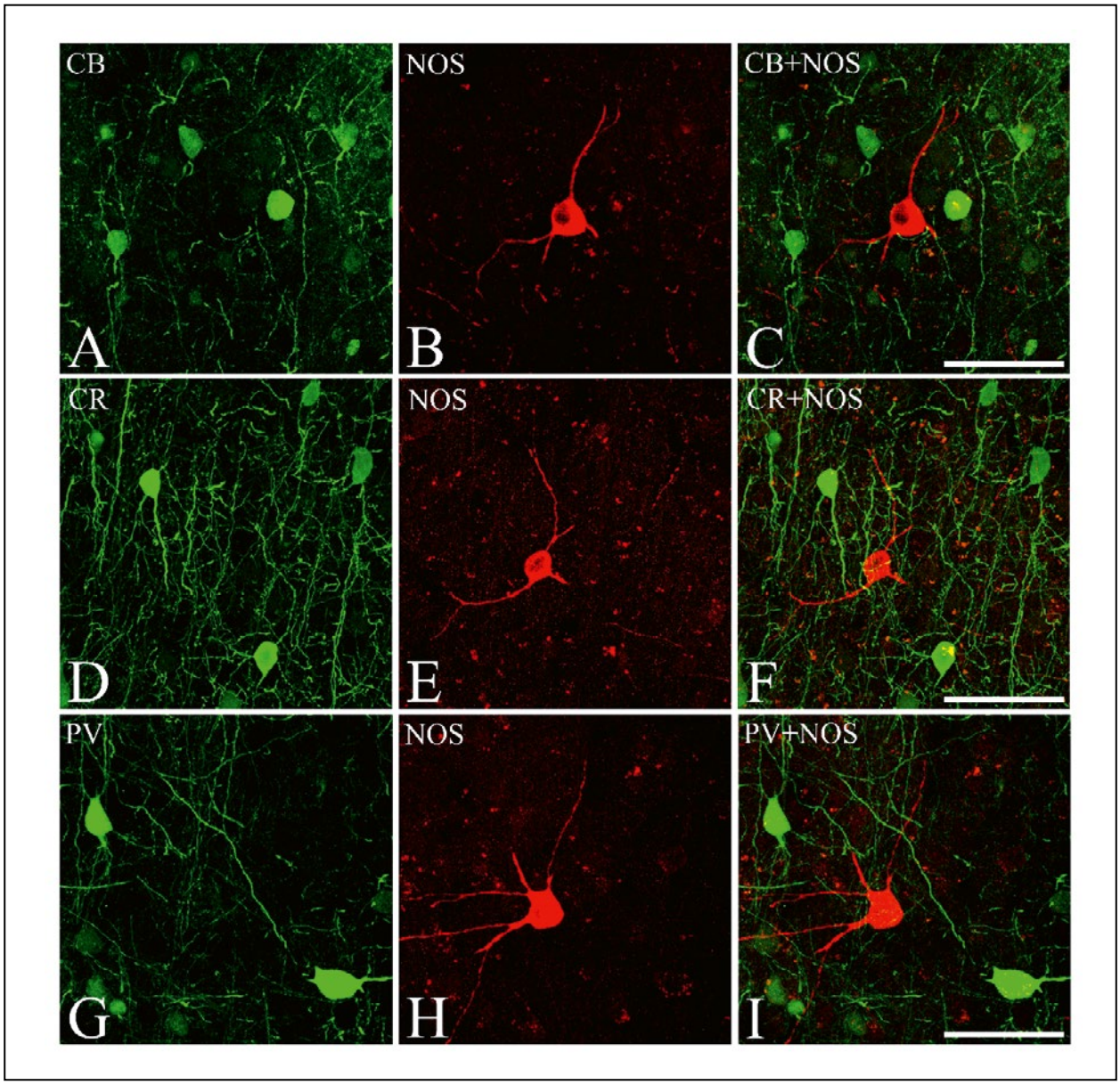

Figure 8. Fluorescence confocal photomicrographs of the gerbil visual cortex immunostained for calcium-binding proteins (CBPs) (A, D, G) or NOS (B, E, H), and superimposed images of CBP and NOS staining (C, F, I). None of the CB-, CR-, and PV-IR neurons expressed NOS. Abbreviations: as in the description of Fig. 1. Scale bar = 50 μm.

expression ratios of GABA in a variety of CB-, CR-, and PV-IR neurons across different brain areas and species. Although the physiological significance of the interspecies and interregional differences in the differential expressional pattern of GABA in CB-, CR-, and PV-IR neurons is not yet fully understood, it appears that the contribution of GABA signaling to CBP-containing neurons might be very diverse.

Based on the expression patterns of various neuronal markers, including CR and PV, at least 13 distinct groups of GABAergic neurons were identified in the mouse visual cortex [72]. In fact, it has been predicted that there are 1,000 different types of neurons present in the visual cortex [99]. In the retina, a recent study revealed 32 functionally different [120] and 46 transcriptionally distinct types [121] of retinal ganglion cells. Moreover, approximately 10 different subtypes of CB- [102], CR- [103, 104], and PV- [105, 106] containing retinal ganglion cells have been identified. These findings indicate that a diversity of cell subtypes work together in concert. To fully understand how the brain mediates visual processing, more information on function, connection, neurochemical processing, and morphology of the diverse subsets of neurons will be required.

In the present study, CB-, CR-, and PV-IR neurons did not contain NOS in the gerbil visual cortex. In accordance with the present study, CB-, CR-, and PV-IR neurons in the bat visual cortex also do not express NOS [73]. In the rat visual cortex, CR- and PV-IR neurons do not coexpress NOS, and it is only found in 1% of CB-IR neurons [56]. However, there are large differences in the expression patterns of NOS in CBP-IR neurons, even among rodent species. For example, 16.7% of CB-IR neurons, 51.7% of CR-IR neurons, and 25.0% of PV-IR neurons in the mouse visual cortex contain NOS [76]. Similarly, 14.7% of CB-IR neurons and 27.5% of CR-IR neurons in the hamster visual cortex contain NOS [54]. In the rabbit visual cortex, 92.4% of CB-IR neurons and 2.5% of CR-IR neurons coexpress NOS, whereas the PV-IR neurons do not [76]. These results show the variable expression patterns of NOS in CBP-IR neurons in the visual cortex between species.

The expression pattern of NOS in CBP-IR neurons is also different in other brain areas. For example, CB--containing neurons in the somatosensory cortex of the mouse [78], CR-containing neurons in the neocortex of the mouse, rat, guinea-pig, rabbit, cat, and monkey [122], and in the rat claustrum [75], and PV-containing neurons in the somatosensory cortex of the mouse [78], the cerebral cortex of the rat [85], neocortices of mouse, rat, guinea-pig, rabbit, cat, and monkey [122], and periaqueductal gray matter of the rat [84] do not contain NOS. However, NOS was found in a minority of CB-containing cells in the cerebral cortex of rats [85], some CB-containing cells in the neocortices of mice, rats, guinea pigs, rabbits, cats, and monkeys [122], and about 20% of CB-containing cells in the cerebral cortices of monkeys [80]. Additionally, NOS is found in 1.93% of CB-containing cells in the mouse basolateral amygdala [123], a minority of CB-containing cells in the rat claustrum [75], and 24–34% of CB-containing cells in rat periaqueductal gray matter [84]. NOS was contained in 8.2% of CR-containing cells in the somatosensory cortex of the mouse [78], 42–49% of CR-containing cells in the hippocampus of the mouse [86], 36–42% of CR-containing cells in the hippocampus of the rat [87], 7.25% of CR-containing cells in the mouse basolateral amygdala [123], and 24.4% of CR-containing cells in the rat dentate gyrus [77]. Finally, NOS was contained in 25.25% of PV-containing cells in the mouse basolateral amygdala [123], a minority of PV-containing cells in the rat claustrum [75], and 1.8% of PV-containing cells in the rat dentate gyrus [77]. However, the functional significance of these variable expressions among different species, in different locations of the brain, is not yet fully understood. They might help elucidate the diversity and functional variation of NOS between species. The lack of colocalization of CB-, CR-, and PV-IR neurons with NOS in the present study suggests that these neurons are anatomically and functionally independent from subgroups of NOS-IR neurons in the gerbil visual cortex.

The function of CBPs in visual processing is still not well known, despite their abundant distribution in the visual cortex. For example, CB participates in the regulation of the circadian rhythm that modulates the response to light, notably via Ca^{2+} homeostasis and sensing [47, 48]. A recent study showed that the effect of activating CR+ neurons was inhibitory, whereas CR+ neurons were less selective to orientation and less surround-suppressed than the CR− neurons in the mouse visual cortex. The functional properties of CR+ neurons are distinguishable from those of PV-, somatostatin-, and vasoactive intestinal peptide--containing interneurons in the mouse visual cortex. The CR-containing neurons are also less selective to orientation than PV-containing interneurons in the mouse visual cortex [124]. PV participates in an excitatory visual pathway that mediates behavioral patterns during the detection of looming objects [125, 126]. In addition, PV-expressing neurons target the somatic and perisomatic compartments of pyramidal neurons linearly to transform the visual responses of pyramidal neurons in the mouse visual cortex [127]. However, the morphological heterogeneity of CBP--IR neurons and their further subdivision depending on the expression of various other neurotransmitters and peptides suggest a great diversity of subtypes of CBP-IR neurons. Determining their precise roles thus warrants further investigation.

Although there are still many unknowns regarding the role of CBP, these proteins are closely associated with various neurological disorders. For example, in the human visual cortex, CB- and CR-IR neurons decrease during aging [128]. However, a significant difference is not observed for CB-IR neurons in the visual cortex of patients with schizophrenia [129], and the densities of CB-, CR-, and PV-IR neurons are not significantly altered in the visual cortex of patients with Alzheimer's disease compared to healthy controls [130]. Although the density of CB-, CR-, and PV-IR interneurons does not significantly change in the visual cortex, the expression of PV mRNA is significantly reduced in the setting of dementia with Lewy bodies and significantly increased in Alzheimer's disease [131]. These results suggest that additional studies are required to provide an in-depth understanding of precise CBP functions and relationships with various neurological disorders affecting the visual cortex.

Folia Histochem Cytobiol. 2023
10.5603/FHC.a2023.0010
ISSN 0239-8508, e-ISSN 1897-5631

In conclusion, the present study shows that CB-, CR-, and PV-IR neurons have specific distribution patterns in the gerbil visual cortex, presenting similarities and differences with other animals. These three CBP-IR neuron types mainly displayed a round/oval morphology. The finding that 16.67% of CB-, 14.16% of CR-, and 39.91% of PV-IR neurons in the gerbil visual cortex contained GABA, suggesting that many of the CBP-IR neurons were not GABAergic interneurons. None of the CB-, CR-, or PV-IR neurons contained NOS. Our study provides useful information for a better understanding of the neurochemical heterogeneity of CB-, CR-, and PV-IR cortical interneurons of the diurnal gerbil visual system and for future functional studies investigating visual information processing in these rodents.

Data availability statement

The datasets used and/or analyzed during the current study are available from the corresponding author on reasonable request.

Author contribution

JRS and CJJ designed the research study. JRS and XYK performed the research. JRS and XYK analyzed the data. JRS and CJJ wrote the manuscript. All authors contributed to editorial changes in the manuscript. All authors read and approved the final manuscript.

Conflicts of interest

The authors declare that there are no conflicts of interest.

Acknowledgements

This research was supported by Basic Science Research Program through the National Research Foundation of Korea (NRF) funded by Ministry of Education (NRF-2020R1F1A1069293 and NRF-2016R1A-6A1A05011910).

References

1. Doulberis M, Papaefthymiou A, Polyzos SA, et al. Rodent models of obesity. Minerva Endocrinol. 2020; 45(3): 243–263, doi: 10.23736/S0391-1977.19.03058-X, indexed in Pubmed: 31738033.
2. Hickman DL, Johnson J, Vemulapalli TH, et al. Commonly used animal models. Principles of Animal Research. 2017: 117–175, doi: 10.1016/b978-0-12-802151-4.00007-4.
3. Julander JG, Siddharthan V. Small-animal models of zika virus. J Infect Dis. 2017; 216(suppl_10): S919–S927, doi: 10.1093/infdis/jix465, indexed in Pubmed: 29267919.
4. Mize RR, Jeon CJ, Butler GD, et al. The calcium binding protein calbindin-D 28K reveals subpopulations of projection and interneurons in the cat superior colliculus. J Comp Neurol. 1991; 307(3): 417–436, doi: 10.1002/cne.903070307, indexed in Pubmed: 1713236.
5. Rai V, Moellmer R, Agrawal DK. Clinically relevant experimental rodent models of diabetic foot ulcer. Mol Cell Biochem. 2022; 477(4): 1239–1247, doi: 10.1007/s11010-022-04372-w, indexed in Pubmed: 35089527.
6. Yamaoka S, Banadyga L, Bray M, et al. Small animal models for studying filovirus pathogenesis. Curr Top Microbiol Immunol. 2017; 411: 195–227, doi: 10.1007/82_2017_9, indexed in Pubmed: 28653189.
7. Zan Y, Haag JD, Chen KS, et al. Production of knockout rats using ENU mutagenesis and a yeast-based screening assay. Nat Biotechnol. 2003; 21(6): 645–651, doi: 10.1038/nbt830, indexed in Pubmed: 12754522.
8. Zhao Y, Qu H, Wang Y, et al. Small rodent models of atherosclerosis. Biomed Pharmacother. 2020; 129: 110426, doi: 10.1016/j.biopha.2020.110426, indexed in Pubmed: 32574973.
9. Batchelder M, Keller LS, Sauer MB, L WeG, Stevens KA, Wilson RP. editors. The Laboratory Rabbit, Guinea Pig, Hamster, and Other Rodents. Elsevier. Academic Press, Boston 2012: 1131–1155.
10. Mishra KK, Srivastava S, Aayyagari A, et al. Development of an animal model of Helicobacter pylori (Indian strain) infection. Indian J Gastroenterol. 2019; 38(2): 167–172, doi: 10.1007/s12664-018-0905-2, indexed in Pubmed: 30911993.
11. Ayan A, Pekağırbaş M, Aypak S, et al. Dentostomella translucida (Gerbil Pinworm) Infection in Mongolian Gerbil (Meriones Unguiculatus) Schulz and Krepkorgorskaja, 1932. Turkiye Parazitol Derg. 2018; 42(4): 290–293, doi: 10.5152/tpd.2018.6032, indexed in Pubmed: 30604691.
12. Junaid OQ, Vythilingam I, Khaw LT, et al. Effect of Brugia pahangi co-infection with Plasmodium berghei ANKA in gerbils (Meriones unguiculatus). Parasitol Res. 2020; 119(4): 1301–1315, doi: 10.1007/s00436-020-06632-4, indexed in Pubmed: 32179986.
13. Rivero FD, Saura A, Prucca CG, et al. Disruption of antigenic variation is crucial for effective parasite vaccine. Nat Med. 2010; 16(5): 551–7, 1p following 557, doi: 10.1038/nm.2141, indexed in Pubmed: 20418884.
14. Matas D, Doniger T, Sarid S, et al. Sex differences in testosterone reactivity and sensitivity in a non-model gerbil. Gen Comp Endocrinol. 2020; 291: 113418, doi: 10.1016/j.ygcen.2020.113418, indexed in Pubmed: 32027878.
15. Kim H, Park JHa, Shin MC, et al. Fate of astrocytes in the gerbil hippocampus after transient global cerebral ischemia. Int J Mol Sci. 2019; 20(4), doi: 10.3390/ijms20040845, indexed in Pubmed: 30781368.
16. Wolf DC, Carlton WW, Turek JJ. Experimental renal papillary necrosis in the Mongolian gerbil (Meriones unguiculatus). Toxicol Pathol. 1992; 20(3 Pt 1): 341–349, doi: 10.1177/019262339202000304, indexed in Pubmed: 1295065.
17. Gouaref I, Detaille D, Wiernsperger N, et al. The desert gerbil Psammomys obesus as a model for metformin-sensitive nutritional type 2 diabetes to protect hepatocellular metabolic damage: Impact of mitochondrial redox state. PLoS One. 2017; 12(2): e0172053, doi: 10.1371/journal.pone.0172053, indexed in Pubmed: 28222147.
18. Quintar AA, Gonçalves BF, Taboga SR, et al. The mongolian gerbil (Meriones unguiculatus) as a model for inflammation-promoted prostate carcinogenesis. Cell Biol Int. 2017; 41(11): 1234–1238, doi: 10.1002/cbin.10789, indexed in Pubmed: 28493535.

19. Bytyqi AH, Layer PG. Lamina formation in the Mongolian gerbil retina (Meriones unguiculatus). Anat Embryol (Berl). 2005; 209(3): 217–225, doi: 10.1007/s00429-004-0443-9, indexed in Pubmed: 15668778.
20. Pan Y, Zhu Q, Xu T, et al. Aggressive behavior and brain neuronal activation in sexually naïve male Mongolian gerbils. Behav Brain Res. 2020; 378: 112276, doi: 10.1016/j.bbr.2019.112276, indexed in Pubmed: 31589893.
21. Bertorelli R, Adami M, Ongini E. The Mongolian gerbil in experimental epilepsy. Ital J Neurol Sci. 1995; 16(1-2): 101–106, doi: 10.1007/BF02229081, indexed in Pubmed: 7642342.
22. Dam AM. Estimation of the total number of neurons in different brain areas in the Mongolian gerbil: a model of experimental ischemia. Acta Neurol Scand Suppl. 1992; 137: 34–36, doi: 10.1111/j.1600-0404.1992.tb05035.x, indexed in Pubmed: 1414259.
23. Kirino T. Delayed neuronal death in the gerbil hippocampus following ischemia. Brain Res. 1982; 239(1): 57–69, doi: 10.1016/0006-8993(82)90833-2, indexed in Pubmed: 7093691.
24. Lee CH, Lee TK, Kim DW, et al. Relationship between neuronal damage/death and astrogliosis in the cerebral motor cortex of gerbil models of mild and severe ischemia and reperfusion injury. Int J Mol Sci. 2022; 23(9), doi: 10.3390/ijms23095096, indexed in Pubmed: 35563487.
25. Ahn JiH, Choi JH, Park JHa, et al. Long-Term exercise improves memory deficits via restoration of myelin and microvessel damage, and enhancement of neurogenesis in the aged gerbil hippocampus after ischemic stroke. Neurorehabil Neural Repair. 2016; 30(9): 894–905, doi: 10.1177/1545968316638444, indexed in Pubmed: 27026692.
26. Bäuerle P, von der Behrens W, Kössl M, et al. Stimulus-specific adaptation in the gerbil primary auditory thalamus is the result of a fast frequency-specific habituation and is regulated by the corticofugal system. J Neurosci. 2011; 31(26): 9708–9722, doi: 10.1523/JNEUROSCI.5814-10.2011, indexed in Pubmed: 21715636.
27. Macharadze T, Budinger E, Brosch M, et al. Early sensory loss alters the dendritic branching and spine density of supragranular pyramidal neurons in rodent primary sensory cortices. Front Neural Circuits. 2019; 13: 61, doi: 10.3389/fncir.2019.00061, indexed in Pubmed: 31611778.
28. Cheng S, Fu Y, Zhang Y, et al. Enhancement of de novo sequencing, assembly and annotation of the Mongolian gerbil genome with transcriptome sequencing and assembly from several different tissues. BMC Genomics. 2019; 20(1): 903, doi: 10.1186/s12864-019-6276-y, indexed in Pubmed: 31775624.
29. Zorio DAR, Monsma S, Sanes DH, et al. De novo sequencing and initial annotation of the Mongolian gerbil (Meriones unguiculatus) genome. Genomics. 2019; 111(3): 441–449, doi: 10.1016/j.ygeno.2018.03.001, indexed in Pubmed: 29526484.
30. Nilsson P, Solbakken MH, Schmid BV, et al. The genome of the great gerbil reveals species-specific duplication of an MHCII gene. Genome Biol Evol. 2020; 12(2): 3832–3849, doi: 10.1093/gbe/evaa008, indexed in Pubmed: 31971556.
31. Kim EB, Lee SG. The complete mitochondrial genome of the Mongolian gerbil, Meriones unguiculatus (Rodentia: Muridae: Gerbillinae). Mitochondrial DNA A DNA Mapp Seq Anal. 2016; 27(2): 1457–1458, doi: 10.3109/19401736.2014.953091, indexed in Pubmed: 25185794.
32. Li CL, Wang CL, Yan SS, et al. The complete mitochondrial genome of the Tamarisk gerbil, (Rodentia: Muridae). Mitochondrial DNA B Resour. 2017; 1(1): 958–959, doi: 10.1080/23802359.2016.1247662, indexed in Pubmed: 33473691.
33. Wang Y, Zhao P, Song Z, et al. Generation of Gene-Knockout Mongolian Gerbils via CRISPR/Cas9 System. Front Bioeng Biotechnol. 2020; 8: 780, doi: 10.3389/fbioe.2020.00780, indexed in Pubmed: 32733872.
34. Govardovskii VI, Röhlich P, Szél A, et al. Cones in the retina of the Mongolian gerbil, Meriones unguiculatus: an immunocytochemical and electrophysiological study. Vision Res. 1992; 32(1): 19–27, doi: 10.1016/0042-6989(92)90108-u, indexed in Pubmed: 1502806.
35. Garcia Garrido M, Beck SC, Mühlfriedel R, et al. Towards a quantitative OCT image analysis. PLoS One. 2014; 9(6): e100080, doi: 10.1371/journal.pone.0100080, indexed in Pubmed: 24927180.
36. Huber G, Heynen S, Imsand C, et al. Novel rodent models for macular research. PLoS One. 2010; 5(10): e13403, doi: 10.1371/journal.pone.0013403, indexed in Pubmed: 20976212.
37. Henschke JU, Noesselt T, Scheich H, et al. Possible anatomical pathways for short-latency multisensory integration processes in primary sensory cortices. Brain Struct Funct. 2015; 220(2): 955–977, doi: 10.1007/s00429-013-0694-4, indexed in Pubmed: 24384580.
38. Rübsamen R, Gutowski M, Langkau J, et al. Growth of central nervous system auditory and visual nuclei in the postnatal gerbil (Meriones unguiculatus). J Comp Neurol. 1994; 346(2): 289–305, doi: 10.1002/cne.903460208, indexed in Pubmed: 7962720.
39. Ellard CG, Goodale MA, Scorfield DM, et al. Visual cortical lesions abolish the use of motion parallax in the Mongolian gerbil. Exp Brain Res. 1986; 64(3): 599–602, doi: 10.1007/BF00340498, indexed in Pubmed: 3803494.
40. Mlinar EJ, Goodale MA. Cortical and tectal control of visual orientation in the gerbil: evidence for parallel channels. Exp Brain Res. 1984; 55(1): 33–48, doi: 10.1007/BF00240496, indexed in Pubmed: 6745353.
41. Hwang IK, Yoo KY, Kim DS, et al. Comparative study on calretinin immunoreactivity in gerbil and rat retina. Anat Histol Embryol. 2005; 34(2): 129–131, doi: 10.1111/j.1439-0264.2004.00583.x, indexed in Pubmed: 15771676.
42. Lee MJ, Lee WT, Jeon CJ. Organization of Neuropeptide Y-Immunoreactive Cells in the Mongolian gerbil () Visual Cortex. Cells. 2021; 10(2), doi: 10.3390/cells10020311, indexed in Pubmed: 33546356.
43. Baimbridge KG, Celio MR, Rogers JH. Calcium-binding proteins in the nervous system. Trends Neurosci. 1992; 15(8): 303–308, doi: 10.1016/0166-2236(92)90081-i, indexed in Pubmed: 1384200.
44. Kovács-Öller T, Szarka G, Ganczer A, et al. Expression of Ca(2+)-binding buffer proteins in the human and mouse retinal neurons. Int J Mol Sci. 2019; 20(9), doi: 10.3390/ijms20092229, indexed in Pubmed: 31067641.
45. Schäfer BW, Heizmann CW. The S100 family of EF-hand calcium-binding proteins: functions and pathology. Trends Biochem Sci. 1996; 21(4): 134–140, doi: 10.1016/s0968-0004(96)80167-8, indexed in Pubmed: 8701470.
46. Schwaller B. Cytosolic Ca(2+) buffers are inherently ca signal modulators. Cold Spring Harb Perspect Biol. 2020; 12(1), doi: 10.1101/cshperspect.a035543, indexed in Pubmed: 31308146.
47. Kriegsfeld LJ, Mei DF, Yan L, et al. Targeted mutation of the calbindin D28K gene disrupts circadian rhythmicity and entrainment. Eur J Neurosci. 2008; 27(11): 2907–2921, doi: 10.1111/j.1460-9568.2008.06239.x, indexed in Pubmed: 18588531.
48. Stadler F, Schmutz I, Schwaller B, et al. Lack of calbindin-D28k alters response of the murine circadian clock to light. Chronobiol Int. 2010; 27(1): 68–82, doi: 10.3109/07420521003648554, indexed in Pubmed: 20205558.

49. Camp AJ, Wijesinghe R. Calretinin: modulator of neuronal excitability. Int J Biochem Cell Biol. 2009; 41(11): 2118–2121, doi: 10.1016/j.biocel.2009.05.007, indexed in Pubmed: 19450707.
50. Kang KW, Pangeni R, Park J, et al. Selective loss of calretinin-poor cochlear afferent nerve fibers in streptozotocin-induced hyperglycemic mice. J Nanosci Nanotechnol. 2020; 20(9): 5515–5519, doi: 10.1166/jnn.2020.17654, indexed in Pubmed: 32331128.
51. Agetsuma M, Hamm JP, Tao K, et al. Parvalbumin-positive interneurons regulate neuronal ensembles in visual cortex. Cereb Cortex. 2018; 28(5): 1831–1845, doi: 10.1093/cercor/bhx169, indexed in Pubmed: 29106504.
52. Permyakov EA, Uversky VN, Permyakov SE. Parvalbumin as a pleomorphic protein. Curr Protein Pept Sci. 2017; 18(8): 780–794, doi: 10.2174/1389203717666161213115746, indexed in Pubmed: 27964700.
53. Park HJ, Kong JH, Kang YS, et al. The distribution and morphology of calbindin D28K- and calretinin-immunoreactive neurons in the visual cortex of mouse. Mol Cells. 2002; 14(1): 143–149, indexed in Pubmed: 12243344.
54. Lee JE, Ahn CH, Lee JY, et al. Nitric oxide synthase and calcium-binding protein-containing neurons in the hamster visual cortex. Mol Cells. 2004; 18(1): 30–39, indexed in Pubmed: 15359121.
55. Kim HG, Gu YN, Lee KP, et al. Immunocytochemical localization of the calcium-binding proteins calbindin D28K, calretinin, and parvalbumin in bat visual cortex. Histol Histopathol. 2016; 31(3): 317–327, doi: 10.14670/HH-11-680, indexed in Pubmed: 26536416.
56. Gonchar Y, Burkhalter A. Three distinct families of GABAergic neurons in rat visual cortex. Cereb Cortex. 1997; 7(4): 347–358, doi: 10.1093/cercor/7.4.347, indexed in Pubmed: 9177765.
57. Park HJ, Lee SN, Lim HR, et al. Calcium-binding proteins calbindin D28K, calretinin, and parvalbumin immunoreactivity in the rabbit visual cortex. Mol Cells. 2000; 10(2): 206–212, doi: 10.1007/s10059-000-0206-2, indexed in Pubmed: 10850663.
58. Jeon CJ, Park HJ. Immunocytochemical localization of calcium-binding protein calretinin containing neurons in cat visual cortex. Mol Cells. 1997; 7(6): 721–725, indexed in Pubmed: 9509411.
59. Yu SH, Lee JY, Jeon CJ. Immunocytochemical localization of calcium-binding proteins, calbindin D28K-, calretinin-, and parvalbumin-containing neurons in the dog visual cortex. Zoolog Sci. 2011; 28(9): 694–702, doi: 10.2108/zsj.28.694, indexed in Pubmed: 21882959.
60. Hendrickson AE, Van Brederode JF, Mulligan KA, et al. Development of the calcium-binding protein parvalbumin and calbindin in monkey striate cortex. J Comp Neurol. 1991; 307(4): 626–646, doi: 10.1002/cne.903070409, indexed in Pubmed: 1651352.
61. Meskenaite V. Calretinin-immunoreactive local circuit neurons in area 17 of the cynomolgus monkey, Macaca fascicularis. J Comp Neurol. 1997; 379(1): 113–132, indexed in Pubmed: 9057116.
62. Glezer II, Hof PR, Morgane PJ. Calretinin-immunoreactive neurons in the primary visual cortex of dolphin and human brains. Brain Res. 1992; 595(2): 181–188, doi: 10.1016/0006-8993(92)91047-i, indexed in Pubmed: 1467964.
63. Leuba G, Saini K. Calcium-binding proteins immunoreactivity in the human subcortical and cortical visual structures. Vis Neurosci. 1996; 13(6): 997–1009, doi: 10.1017/s0952523800007665, indexed in Pubmed: 8961531.
64. Picón-Pagès P, Garcia-Buendia J, Muñoz FJ. Functions and dysfunctions of nitric oxide in brain. Biochim Biophys Acta Mol Basis Dis. 2019; 1865(8): 1949–1967, doi: 10.1016/j.bbadis.2018.11.007, indexed in Pubmed: 30500433.
65. Lundberg JO, Weitzberg E. Nitric oxide signaling in health and disease. Cell. 2022; 185(16): 2853–2878, doi: 10.1016/j.cell.2022.06.010, indexed in Pubmed: 35931019.
66. Zhou Li, Zhu DY. Neuronal nitric oxide synthase: structure, subcellular localization, regulation, and clinical implications. Nitric Oxide. 2009; 20(4): 223–230, doi: 10.1016/j.niox.2009.03.001, indexed in Pubmed: 19298861.
67. Förstermann U, Sessa WC. Nitric oxide synthases: regulation and function. Eur Heart J. 2012; 33(7): 829–37, 837a, doi: 10.1093/eurheartj/ehr304, indexed in Pubmed: 21890489.
68. Kourosh-Arami M, Hosseini N, Mohsenzadegan M, et al. Neurophysiologic implications of neuronal nitric oxide synthase. Rev Neurosci. 2020; 31(6): 617–636, doi: 10.1515/revneuro-2019-0111, indexed in Pubmed: 32739909.
69. Choi S, Won JS, Carroll SL, et al. Pathology of nNOS-Expressing GABAergic Neurons in Mouse Model of Alzheimer's Disease. Neuroscience. 2018; 384: 41–53, doi: 10.1016/j.neuroscience.2018.05.013, indexed in Pubmed: 29782905.
70. Dawson VL, Dawson TM. Nitric oxide in neurodegeneration. Prog Brain Res. 1998; 118: 215–229, doi: 10.1016/s0079-6123(08)63210-0, indexed in Pubmed: 9932444.
71. Poon CH, Tsui KaC, Chau SC, et al. Functional roles of neuronal nitric oxide synthase in neurodegenerative diseases and mood disorders. Curr Alzheimer Res. 2021; 18(10): 831–840, doi: 10.2174/1567205018666211022164025, indexed in Pubmed: 34719364.
72. Gonchar Y, Wang Q, Burkhalter A. Multiple distinct subtypes of GABAergic neurons in mouse visual cortex identified by triple immunostaining. Front Neuroanat. 2007; 1: 3, doi: 10.3389/neuro.05.003.2007, indexed in Pubmed: 18958197.
73. Gu YN, Kim HG, Jeon CJ. Localization of nitric oxide synthase-containing neurons in the bat visual cortex and co-localization with calcium-binding proteins. Acta Histochem Cytochem. 2015; 48(4): 125–133, doi: 10.1267/ahc.14066, indexed in Pubmed: 26379314.
74. Kim IB, Oh SJ, Chun MH. Neuronal nitric oxide synthase immunoreactive neurons in the mammalian retina. Microscopy Research and Technique. 2000; 50(2): 112–123, doi: 10.1002/1097-0029(20000715)50:2<112::aid-jemt3>3.0.co;2-s.
75. Kowiański P, Moryś JM, Wójcik S, et al. Co-localisation of NOS with calcium-binding proteins during the postnatal development of the rat claustrum. Folia Morphol (Warsz). 2003; 62(3): 211–214, indexed in Pubmed: 14507049.
76. Lee JE, Jeon CJ. Immunocytochemical localization of nitric oxide synthase-containing neurons in mouse and rabbit visual cortex and co-localization with calcium-binding proteins. Mol Cells. 2005; 19(3): 408–417, indexed in Pubmed: 15995359.
77. Liang Z, Zhang L, Wang X, et al. Distribution and neurochemical features of neuronal nitric oxide synthase-expressing interneurons in the rat dentate gyrus. Brain Res. 2013; 1505: 11–21, doi: 10.1016/j.brainres.2013.02.014, indexed in Pubmed: 23419891.
78. Magno L, Oliveira MG, Mucha M, et al. Multiple embryonic origins of nitric oxide synthase-expressing GABAergic neurons of the neocortex. Front Neural Circuits. 2012; 6: 65, doi: 10.3389/fncir.2012.00065, indexed in Pubmed: 23015780.
79. Mendez-Otero R, Tenorio F, Giraldi-Guimarães A, et al. Patterns of nitric oxide synthase expression in the developing superior colliculus. Rev Bras Biol. 1996; 56(Suppl. 1 pt. 1): 113–122, indexed in Pubmed: 9394494.
80. Smiley JF, McGinnis JP, Javitt DC. Nitric oxide synthase interneurons in the monkey cerebral cortex are subsets of the somatostatin, neuropeptide Y, and calbindin cells. Brain Res. 2000; 863(1-2): 205–212, doi: 10.1016/s0006-8993(00)02136-3, indexed in Pubmed: 10773208.
81. Yousef T, Neubacher U, Eysel UT, et al. Nitric oxide synthase in rat visual cortex: an immunohistochemical study. Brain Res

Brain Res Protoc. 2004; 13(1): 57–67, doi: 10.1016/j.brainresprot.2004.01.004, indexed in Pubmed: 15063842.
82. Daff S. Calmodulin-dependent regulation of mammalian nitric oxide synthase. Biochem Soc Trans. 2003; 31(Pt 3): 502–505, doi: 10.1042/bst0310502, indexed in Pubmed: 12773144.
83. Piazza M, Guillemette JG, Dieckmann T. Dynamics of nitric oxide synthase-calmodulin interactions at physiological calcium concentrations. Biochemistry. 2015; 54(11): 1989–2000, doi: 10.1021/bi501353s, indexed in Pubmed: 25751535.
84. Barbaresi P, Mensà E, Lariccia V, et al. Differential distribution of parvalbumin- and calbindin-D28K-immunoreactive neurons in the rat periaqueductal gray matter and their colocalization with enzymes producing nitric oxide. Brain Res Bull. 2013; 99: 48–62, doi: 10.1016/j.brainresbull.2013.09.004, indexed in Pubmed: 24107244.
85. Bertini G, Peng ZC, Bentivoglio M. The chemical heterogeneity of cortical interneurons: nitric oxide synthase vs. calbindin and parvalbumin immunoreactivity in the rat. Brain Res Bull. 1996; 39(4): 261–266, doi: 10.1016/0361-9230(95)02133-7, indexed in Pubmed: 8963693.
86. Jinno S, Kinukawa N, Kosaka T. Morphometric multivariate analysis of GABAergic neurons containing calretinin and neuronal nitric oxide synthase in the mouse hippocampus. Brain Res. 2001; 900(2): 195–204, doi: 10.1016/s0006-8993(01)02292-2, indexed in Pubmed: 11334798.
87. Megías M, Verduga R, Fernández-Viadero C, et al. Neurons co-localizing calretinin immunoreactivity and reduced nicotinamide adenine dinucleotide phosphate diaphorase (NADPH-d) activity in the hippocampus and dentate gyrus of the rat. Brain Res. 1997; 744(1): 112–120, doi: 10.1016/s0006-8993(96)01075-x, indexed in Pubmed: 9030419.
88. Soares-Mota M, Henze I, Mendez-Otero R. Nitric oxide synthase-positive neurons in the rat superior colliculus: colocalization of NOS with NMDAR1 glutamate receptor, GABA, and parvalbumin. J Neurosci Res. 2001; 64(5): 501–507, doi: 10.1002/jnr.1102, indexed in Pubmed: 11391705.
89. Dun NJ, Huang R, Dun SL, et al. Infrequent co-localization of nitric oxide synthase and calcium binding proteins immunoreactivity in rat neocortical neurons. Brain Res. 1994; 666(2): 289–294, doi: 10.1016/0006-8993(94)90786-2, indexed in Pubmed: 7533636.
90. González-Albo MC, Elston GN, DeFelipe J. The human temporal cortex: characterization of neurons expressing nitric oxide synthase, neuropeptides and calcium-binding proteins, and their glutamate receptor subunit profiles. Cereb Cortex. 2001; 11(12): 1170–1181, doi: 10.1093/cercor/11.12.1170, indexed in Pubmed: 11709488.
91. Druga R. Neocortical inhibitory system. Folia Biol (Praha). 2009; 55(6): 201–217, indexed in Pubmed: 20163769.
92. Watanabe M, Maemura K, Kanbara K, et al. GABA and GABA receptors in the central nervous system and other organs. Int Rev Cytol. 2002; 213: 1–47, doi: 10.1016/s0074-7696(02)13011-7, indexed in Pubmed: 11837891.
93. Ichida JM, Rosa M, Casagrande VA. Does the visual system of the flying fox resemble that of primates? The distribution of calcium-binding proteins in the primary visual pathway of Pteropus poliocephalus. J Comp Neurol. 2000; 417(1): 73–87, doi: 10.1002/(sici)1096-9861(20000131)417:1<73::aid-cne6>3.0.co;2-c, indexed in Pubmed: 10660889.
94. Stichel CC, Singer W, Heizmann CW, et al. Immunohistochemical localization of calcium-binding proteins, parvalbumin and calbindin-D 28k, in the adult and developing visual cortex of cats: a light and electron microscopic study. J Comp Neurol. 1987; 262(4): 563–577, doi: 10.1002/cne.902620409, indexed in Pubmed: 3667965.
95. Goodchild AK, Martin PR. The distribution of calcium-binding proteins in the lateral geniculate nucleus and visual cortex of a New World monkey, the marmoset, Callithrix jacchus. Vis Neurosci. 1998; 15(4): 625–642, doi: 10.1017/s0952523898154044, indexed in Pubmed: 9682866.
96. Demeulemeester H, Arckens L, Vandesande F, et al. Calcium binding proteins and neuropeptides as molecular markers of GABAergic interneurons in the cat visual cortex. Exp Brain Res. 1991; 84(3): 538–544, doi: 10.1007/BF00230966, indexed in Pubmed: 1864325.
97. Park HJ, Hong SK, Kong JH, et al. Localization of calcium-binding protein parvalbumin-immunoreactive neurons in mouse and hamster visual cortex. Mol Cell. 1999; 9(5): 542–547, indexed in Pubmed: 10597044.
98. Blümcke I, Hof PR, Morrison JH, et al. Distribution of parvalbumin immunoreactivity in the visual cortex of Old World monkeys and humans. J Comp Neurol. 1990; 301(3): 417–432, doi: 10.1002/cne.903010307, indexed in Pubmed: 2262599.
99. Masland RH. Neuronal cell types. Curr Biol. 2004; 14(13): R497–R500, doi: 10.1016/j.cub.2004.06.035, indexed in Pubmed: 15242626.
100. Wang Y, Toledo-Rodriguez M, Gupta A, et al. Anatomical, physiological and molecular properties of Martinotti cells in the somatosensory cortex of the juvenile rat. J Physiol. 2004; 561 (Pt 1): 65–90, doi: 10.1113/jphysiol.2004.073353, indexed in Pubmed: 15331670.
101. Hayes TL, Lewis DA. Nonphosphorylated neurofilament protein and calbindin immunoreactivity in layer III pyramidal neurons of human neocortex. Cereb Cortex. 1992; 2(1): 56–67, doi: 10.1093/cercor/2.1.56, indexed in Pubmed: 1633408.
102. Gu YN, Lee ES, Jeon CJ. Types and density of calbindin D28k-immunoreactive ganglion cells in mouse retina. Exp Eye Res. 2016; 145: 327–336, doi: 10.1016/j.exer.2016.02.001, indexed in Pubmed: 26874036.
103. Kwon OJ, Lee ES, Jeon CJ. Density and types of calretinin-containing retinal ganglion cells in rabbit. Neuroscience. 2014; 278: 343–353, doi: 10.1016/j.neuroscience.2014.08.025, indexed in Pubmed: 25168727.
104. Lee ES, Lee JY, Jeon CJ. Types and density of calretinin--containing retinal ganglion cells in mouse. Neurosci Res. 2010; 66(2): 141–150, doi: 10.1016/j.neures.2009.10.008, indexed in Pubmed: 19895859.
105. Kim TJ, Jeon CJ. Morphological classification of parvalbumin--containing retinal ganglion cells in mouse: single-cell injection after immunocytochemistry. Invest Ophthalmol Vis Sci. 2006; 47(7): 2757–2764, doi: 10.1167/iovs.05-1442, indexed in Pubmed: 16799011.
106. Lee ES, Kim TJ, Jeon CJ. Identification of parvalbumin--containing retinal ganglion cells in rabbit. Exp Eye Res. 2013; 110: 113–124, doi: 10.1016/j.exer.2013.02.018, indexed in Pubmed: 23518406.
107. Lee JY, Choi JS, Ye EA, et al. Organization of calbindin D28K-immunoreactive neurons in the dog superior colliculus. Zoolog Sci. 2007; 24(11): 1103–1114, doi: 10.2108/zsj.24.1103, indexed in Pubmed: 18348611.
108. Jeon CJ, Pyun JK, Yang HW. Calretinin and calbindin D28K immunoreactivity in the superficial layers of the rabbit superior colliculus. Neuroreport. 1998; 9(17): 3847–3852, doi: 10.1097/00001756-199812010-00015, indexed in Pubmed: 9875716.
109. Lee JY, Choi JS, Ahn CH, et al. Calcium-binding protein calretinin immunoreactivity in the dog superior colliculus. Acta Histochem Cytochem. 2006; 39(5): 125–138, doi: 10.1267/ahc.06008, indexed in Pubmed: 17327899.

110. Ellias SA, Stevens JK. The dendritic varicosity: a mechanism for electrically isolating the dendrites of cat retinal amacrine cells? Brain Res. 1980; 196(2): 365–372, doi: 10.1016/0006-8993(80)90401-1, indexed in Pubmed: 6249448.
111. Gu Y, Jukkola P, Wang Q, et al. Polarity of varicosity initiation in central neuron mechanosensation. J Cell Biol. 2017; 216(7): 2179–2199, doi: 10.1083/jcb.201606065, indexed in Pubmed: 28606925.
112. Gu C. Rapid and reversible development of axonal varicosities: a new form of neural plasticity. Front Mol Neurosci. 2021; 14: 610857, doi: 10.3389/fnmol.2021.610857, indexed in Pubmed: 33613192.
113. Liebert AD, Chow RT, Bicknell BT, et al. Neuroprotective effects against POCD by photobiomodulation: evidence from assembly/disassembly of the cytoskeleton. J Exp Neurosci. 2016; 10: 1–19, doi: 10.4137/JEN.S33444, indexed in Pubmed: 26848276.
114. Ralevic V. History of geoff burnstock's research on P2 receptors. Biochem Pharmacol. 2021; 187: 114358, doi: 10.1016/j.bcp.2020.114358, indexed in Pubmed: 33279495.
115. Zhang ZW, Kang JIl, Vaucher E. Axonal varicosity density as an index of local neuronal interactions. PLoS One. 2011; 6(7): e22543, doi: 10.1371/journal.pone.0022543, indexed in Pubmed: 21811630.
116. Villalobos CA, Wu Q, Lee PH, et al. Parvalbumin and GABA Microcircuits in the Mouse Superior Colliculus. Front Neural Circuits. 2018; 12: 35, doi: 10.3389/fncir.2018.00035, indexed in Pubmed: 29780307.
117. Jeong SJ, Kim HH, Lee WS, et al. Immunocytochemical localization of calbindin D28K, calretinin, and parvalbumin in bat superior colliculus. Acta Histochem Cytochem. 2014; 47(3): 113–123, doi: 10.1267/ahc.14004, indexed in Pubmed: 25320408.
118. Hong SK, Kim JY, Jeon CJ. Immunocytochemical localization of calretinin in the superficial layers of the cat superior colliculus. Neurosci Res. 2002; 44(3): 325–335, doi: 10.1016/s0168-0102(02)00154-2, indexed in Pubmed: 12413661.
119. Lee JY, Jeong SJ, Jeon CJ. Parvalbumin-immunoreactive cells in the superior colliculus in dog: distribution, colocalization with GABA, and effect of monocular enucleation. Zoolog Sci. 2014; 31(11): 748–757, doi: 10.2108/zs140073, indexed in Pubmed: 25366158.
120. Baden T, Berens P, Franke K, et al. The functional diversity of retinal ganglion cells in the mouse. Nature. 2016; 529(7586): 345–350, doi: 10.1038/nature16468, indexed in Pubmed: 26735013.
121. Tran NM, Shekhar K, Whitney IE, et al. Single-cell profiles of retinal ganglion cells differing in resilience to injury reveal neuroprotective genes. Neuron. 2019; 104(6): 1039–1055.e12, doi: 10.1016/j.neuron.2019.11.006, indexed in Pubmed: 31784286.
122. Yan XX, Garey LJ. Morphological diversity of nitric oxide synthesising neurons in mammalian cerebral cortex. J Hirnforsch. 1997; 38(2): 165–172, indexed in Pubmed: 9176729.
123. Wang X, Liu C, Wang X, et al. Density and neurochemical profiles of neuronal nitric oxide synthase-expressing interneuron in the mouse basolateral amygdala. Brain Res. 2017; 1663: 106–113, doi: 10.1016/j.brainres.2017.02.009, indexed in Pubmed: 28213154.
124. Camillo D, Ahmadlou M, Saiepour MH, et al. Visual processing by calretinin expressing inhibitory neurons in mouse primary visual cortex. Sci Rep. 2018; 8(1): 12355, doi: 10.1038/s41598-018-30958-w, indexed in Pubmed: 30120412.
125. Shang C, Chen Z, Liu A, et al. Divergent midbrain circuits orchestrate escape and freezing responses to looming stimuli in mice. Nat Commun. 2018; 9(1): 1232, doi: 10.1038/s41467-018-03580-7, indexed in Pubmed: 29581428.
126. Shang C, Liu Z, Chen Z, et al. BRAIN CIRCUITS. A parvalbumin-positive excitatory visual pathway to trigger fear responses in mice. Science. 2015; 348(6242): 1472–1477, doi: 10.1126/science.aaa8694, indexed in Pubmed: 26113723.
127. Atallah BV, Bruns W, Carandini M, et al. Parvalbumin-expressing interneurons linearly transform cortical responses to visual stimuli. Neuron. 2012; 73(1): 159–170, doi: 10.1016/j.neuron.2011.12.013, indexed in Pubmed: 22243754.
128. Bu J, Sathyendra V, Nagykery N, et al. Age-related changes in calbindin-D28k, calretinin, and parvalbumin-immunoreactive neurons in the human cerebral cortex. Exp Neurol. 2003; 182(1): 220–231, doi: 10.1016/s0014-4886(03)00094-3, indexed in Pubmed: 12821392.
129. Wheeler DG, Dixon G, Harper CG. No differences in calcium-binding protein immunoreactivity in the posterior cingulate and visual cortex: schizophrenia and controls. Prog Neuropsychopharmacol Biol Psychiatry. 2006; 30(4): 630–639, doi: 10.1016/j.pnpbp.2005.11.041, indexed in Pubmed: 16503370.
130. Leuba G, Kraftsik R, Saini K. Quantitative distribution of parvalbumin, calretinin, and calbindin D-28k immunoreactive neurons in the visual cortex of normal and Alzheimer cases. Exp Neurol. 1998; 152(2): 278–291, doi: 10.1006/exnr.1998.6838, indexed in Pubmed: 9710527.
131. Khundakar AA, Hanson PS, Erskine D, et al. Analysis of primary visual cortex in dementia with Lewy bodies indicates GABAergic involvement associated with recurrent complex visual hallucinations. Acta Neuropathol Commun. 2016; 4(1): 66, doi: 10.1186/s40478-016-0334-3, indexed in Pubmed: 27357212.

Submitted: 4 May, 2023
Accepted after reviews: 19 June, 2023
Available as AoP: 6 July, 2023